THE JOURNAL OF PHYSICAL CHEMISTRY C

Article

pubs.acs.org/JPCC

Optimizing C–C Coupling on Oxide-Derived Copper Catalysts for Electrochemical CO_2 Reduction

Yanwei Lum,[†,‡,⊥] Binbin Yue,[Δ,∥] Peter Lobaccaro,[†,§,#] Alexis T. Bell,*[,†,§,#] and Joel W. Ager*[,†,‡,⊥]

[†]Joint Center for Artificial Photosynthesis, [‡]Materials Science Division, [§]Chemical Sciences Division, and [∥]Advanced Light Source, Lawrence Berkeley National Laboratory, Berkeley, California 94720, United States

[⊥]Department of Materials Science and Engineering and [#]Department of Chemical and Biomolecular Engineering, University of California, Berkeley, California 94720, United States

[Δ]Center for High Pressure Science and Technology Advanced Research, 1690 Cailun Road, Pudong, Shanghai 201203, People's Republic of China

Supporting Information

ABSTRACT: Copper electrodes, prepared by reduction of oxidized metallic copper, have been reported to exhibit higher activity for the electrochemical reduction of CO_2 and better selectivity toward C_2 and C_3 (C_{2+}) products than metallic copper that has not been preoxidized. We report here an investigation of the effects of four different preparations of oxide-derived electrocatalysts on their activity and selectivity for CO_2 reduction, with particular attention given to the selectivity to C_{2+} products. All catalysts were tested for CO_2 reduction in 0.1 M $KHCO_3$ and 0.1 M $CsHCO_3$ at applied voltages in the range from −0.7 to −1.0 V vs RHE. The best performing oxide-derived catalysts show up to ∼70% selectivity to C_{2+} products and only ∼3% selectivity to C_1 products at −1.0 V vs RHE when $CsHCO_3$ is used as the electrolyte. In contrast, the selectivity to C_{2+} products decreases to ∼56% for the same catalysts tested in $KHCO_3$. By studying all catalysts under identical conditions, the key factors affecting product selectivity could be discerned. These efforts reveal that the surface area of the oxide-derived layer is a critical parameter affecting selectivity. A high selectivity to C_{2+} products is attained at an overpotential of −1 V vs RHE by operating at a current density sufficiently high to achieve a moderately high pH near the catalyst surface but not so high as to cause a significant reduction in the local concentration of CO_2. On the basis of recent theoretical studies, a high pH suppresses the formation of C_1 relative to C_{2+} products. At the same time, however, a high local CO_2 concentration is necessary for the formation of C_{2+} products.

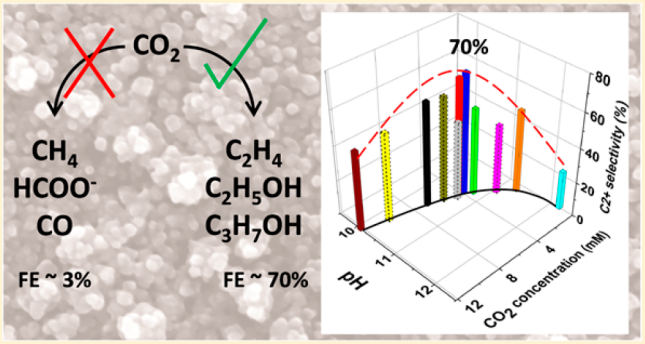

INTRODUCTION

Electrochemical reduction of CO_2 to fuels using renewable electrical energy (e.g., generated by solar radiation or wind) is a potential source of sustainable fuel for the future.[1,2] Pursuit of this option has led to considerable interest in discovering electrocatalysts that can promote electrochemical CO_2 reduction (CO2R) efficiently and with high selectivity to targeted products.[3−5] The main bottleneck has been the catalyst itself, as one does not yet exist that can produce chemical fuels at low overpotential and with high selectivity.[5−9] Of the various metal-based catalysts studied for CO2R, copper remains the only one capable of producing significant amounts of hydrocarbons and oxygenates.[3,4,9] However, the selectivity to any particular product is not especially high.[10] Clearly, improvements in CO2R electrocatalysts are required for this process to be viable for producing renewable fuels. In particular, catalysts are desired for producing ethylene and ethanol, which can be readily converted to fuels.[11]

In recent years, a new class of Cu-based catalysts with higher activity, better C_{2+} selectivity, and lower overpotential requirements for CO2R has emerged.[12−21] These "oxide-derived" catalysts can be prepared via oxidation of Cu via thermal[12−14] or electrochemical[18,22] treatments or by exposure to an O_2 plasma.[20] The oxidized Cu is then reduced back to its metallic form. Kanan and co-workers have shown that growth of thick copper oxide layers by thermal oxidation followed by subsequent reduction produces an electrocatalyst that can promote CO2R at overpotentials less than 0.4 V.[12] Interestingly, when the catalyst is utilized for CO reduction, it is able to generate C_2 and C_3 (C_{2+}) liquid products with up to 57% faradaic efficiency (FE) at an applied potential of only −0.3 V vs RHE.[14] Improved selectivities and lower onset potentials for C_{2+} products also have been reported for oxide-

Received: April 19, 2017
Revised: May 24, 2017
Published: June 12, 2017

DOI: 10.1021/acs.jpcc.7b03673
J. Phys. Chem. C 2017, 121, 14191−14203

derived catalysts made by electrochemical processing and by chemical treatment of copper oxide nanowires.[12−21] Oxidation−reduction processing has also been applied to gold and silver, and decreases in the overpotential required for CO_2 reduction to CO have been reported by a number of groups.[23−27]

There are two important issues not addressed in previous studies of oxide-derived Cu catalysts. The first is the extent to which the performance of such catalysts is influenced by the manner of catalyst preparation and operation. Of particular interest in the latter context is the extent to which the pH and CO_2 concentration near the electrode affect product selectivity. To address these questions, catalysts prepared by different procedures must be tested under strictly identical conditions and in the same electrochemical cell.[28] The second issue is the identity of the electrolyte cation and its effect on catalyst activity and selectivity.[3,29−32] For example, Hori and co-workers have observed that the size of the alkaline metal cation (Li^+, Na^+, K^+, and Cs^+) influences the ratio of C_2/C_1 products formed on metallic Cu at a fixed current density of 5 mA cm^{-2}.[3,31] Use of Cs^+ as the electrolyte cation as compared to a Li^+ resulted in a higher selectivity to C_{2+} products, lower selectivity to hydrogen evolution (HER) and C_1 products, and a lower applied potential requirement for a fixed current density. Kenis and co-workers observed a similar effect for production of CO by CO2R on Ag electrodes, finding larger cations yield higher partial current densities to CO, a lower overpotential for a given current density, and a suppression of the HER.[30]

The present study was undertaken to address the questions posed above. Four representative oxide-derived (OD) copper catalysts were synthesized: "oxide-derived nanocrystalline copper" developed by Kanan and co-workers,[12−14] "Cu nanowire arrays" developed by Smith and co-workers,[15] "electrodeposited copper(I) oxide films" developed by Yeo and co-workers,[16] and "electrochemical oxidation−reduction cycled Cu" developed by Nilsson and co-workers.[18] The performance of these catalysts was examined in both $KHCO_3$ and $CsHCO_3$ electrolytes. The information gained from these investigations, combined with detailed structural characterization of the catalysts, allowed us to identify how catalyst structure and the conditions chosen for CO2R affect catalyst activity and C_{2+} product selectivity. These studies reveal that it is possible to achieve a FE as high as 70% for C_{2+} products. This result is achieved by operating the catalysts at current densities that enable attainment of a high electrolyte pH adjacent to the cathode without excessive lowering of the local concentration of CO_2 due to the reaction of CO_2 with OH^- anions to form HCO_3^- and CO_3^{2-} anions. We show that these conditions can be achieved because the kinetics of the reaction of CO_2 with OH^- anions is slow.[33]

METHODS

Materials. The highest purity reagents were procured wherever possible to mitigate the potential effect of impurities. Cesium carbonate (99.995% metals basis), potassium carbonate (99.995% metals basis), potassium chloride (≥99.9995% metals basis), ammonium persulfate (≥98.0%), sodium hydroxide (99.99% metals basis), lactic acid (≥85%), perchloric acid (60%), nitric acid (70%), hydrochloric acid (37%), and sulfuric acid (99.999% metals basis) were purchased from Sigma-Aldrich. Copper foil (0.1 mm thick, 99.9999% metals basis) and copper(II) sulfate hydrate (99.999% metals basis) were purchased from Alfa Aesar. Phosphoric acid (85.0−87.0% assay) was purchased from J.T. Baker. Gold seal plain microscope glass slides (75 × 25 × 1 mm^3) were purchased from Electron Microscopy Services. Copper slugs (99.999%) and titanium slugs (99.999%) for electron beam evaporation were purchased from Kurt J. Lesker Company. Selemion AMV anionic exchange membranes were purchased from Asahi Glass Co., Ltd. Nafion proton exchange membranes were purchased from Ion Power Inc. All chemicals were used without further purification. Carbon dioxide (99.995%), nitrogen (99.999%), argon (99.999%), and hydrogen (99.999%) were purchased from Praxair. Hydrogen, argon, nitrogen, and carbon dioxide gas purifiers purchased from Valco Instruments Co. Inc. were used on the gas feeds to the electrochemical cell and gas chromatograph. 18.2 MΩ deionized (DI) water was produced by a Millipore system.

Preparation of Cu Foil. Cu foil was electropolished in concentrated phosphoric acid using a two-electrode system at an applied potential of 2 V vs the counter electrode for 5 min. During this procedure, another copper foil was utilized as the counter electrode, and agitation of the solution was created with a magnetic stirrer. The copper foil was then rinsed copiously with DI water and dried with a stream of nitrogen. The copper foil was then sonicated in DI water for 2 min and dried again with a stream of nitrogen.

Preparation of Oxide-Derived Nanocrystalline Copper (OD Cu). Preparation of OD Cu via the thermal annealing process was performed according to the procedure of Kanan and co-workers.[12−14] Copper foil was first electropolished in concentrated phosphoric acid as described above. The electropolished copper foil was then placed in a muffle furnace, which was heated from room temperature to 500 °C at a rate of 10 °C min^{-1} under an air atmosphere. The temperature was maintained at 500 °C for 1 h, which generated a thick oxide, containing both Cu_2O and CuO, on the surface of the foil (XRD pattern in Figure S1a and XPS spectrum in Figure S3a). The copper foil was then allowed to gradually cool to room temperature. The copper oxide layer was then electrochemically reduced before electrolysis by applying a potential of −1.2 V vs Ag/AgCl until complete reduction had taken place (Figure S5a). The XRD pattern, XPS narrow scan of the Cu 2p peak, optical image, and detailed SEM images of fully reduced OD Cu are shown in Figures S2a, S4a, S7, and S8, respectively.

Preparation of Cu Nanowire Arrays (OD NWs). Preparation of OD NWs was performed according to the procedure of Smith and co-workers.[15] Copper foil was first electropolished in concentrated phosphoric acid as described above. The copper foil was then soaked in an aqueous solution containing 0.133 M ammonium persulfate and 2.667 M sodium hydroxide to generate a $CuO/Cu(OH)_2$ nanowire array on the surface (XRD pattern in Figure S1b). Copper foils were soaked for varying times (75, 150, 300, and 600 s), with a longer soaking time generating a denser and longer nanowire array. The copper foils were then rinsed copiously with DI water and dried with a stream of nitrogen. To obtain CuO nanowire arrays, the copper foils were placed in a muffle furnace, which was then heated from room temperature to 150 °C at a rate of 5 °C min^{-1} under an air atmosphere for 2 h (XRD pattern in Figure S1c and XPS spectrum in Figure S3b). The CuO nanowire arrays were then reduced electrochemically before electrolysis by applying a potential of −1.2 V vs Ag/AgCl until complete reduction had taken place (Figure S5b). The XRD pattern, XPS narrow scan of the Cu 2p region, optical image,

DOI: 10.1021/acs.jpcc.7b03673
J. Phys. Chem. C 2017, 121, 14191−14203

and SEM images of the fully reduced OD NWs are shown in Figures S2b, S4b, S7, S9, and S10.

Preparation of Electrochemically Cycled Copper (EC Cu). Preparation of EC Cu was performed according to the procedure of Nilsson and co-workers with some modifications.[18,22] Copper foil was first electropolished in concentrated phosphoric acid as described above. Electrochemical oxidation−reduction cycling of the copper foil was then carried out in a three-electrode system with another copper foil as the working electrode, Pt as the counter electrode, and 0.1 M $KHCO_3$ solution containing 16 mM KCl as the electrolyte. The electrolyte was first saturated with CO_2, and the potential was swept from open circuit voltage to 0.2 V vs Ag/AgCl and then to −1.2 V vs Ag/AgCl for one cycle at a rate of 20 mV s^{-1} (Figure S5d). Sweeping to oxidative potentials generates a Cu_2O layer on the surface (XRD pattern in Figure S1d), which is then subsequently reduced back to metallic Cu at reductive potentials. The copper foil was then rinsed copiously with DI water and dried with a stream of nitrogen. The XRD pattern, XPS narrow scan of the Cu 2p peaks, optical image, and SEM image of the fully reduced EC Cu are shown in Figures S2c, S4c, S7, and S11.

Preparation of Reduced Electrodeposited Cu(I) Oxide Films (EOD Cu). Preparation of EOD Cu was performed according to the procedure of Yeo and co-workers with some modifications.[16] Glass slides (75 × 25 × 1 mm^3) were first cleaned in a custom-made O_2 plasma system for 1 min and subsequently sonicated in DI water for 10 min. The slides were then loaded into an electron beam evaporator where 40 nm of Ti (adhesion layer) and subsequently 100 nm of Cu were deposited. Cu_2O was then electrochemically deposited onto the Cu surface using a two-electrode system with a copper foil as the counter electrode and an aqueous solution containing 0.3 M $CuSO_4$, 3.2 M NaOH, and 2.3 M lactic acid as the electrolyte (Figure S1e). Electrodeposition was performed in a glass cell, and the temperature was controlled with a water bath held at 60 °C with agitation created using a magnetic stirrer. A constant current density of −1.82 mA cm^{-2} was used for deposition, and different thicknesses of Cu_2O were produced by varying the deposition time (50, 100, 200, and 300 s). The Cu_2O layer was then reduced electrochemically before electrolysis by applying a potential of −1.2 V vs Ag/AgCl until complete reduction had taken place (Figure S5c). The XRD pattern, XPS narrow scan of the Cu 2p peaks, optical image, and SEM images are shown in Figures S2d, S4d, S7, S12, and S13.

Material Characterization. X-ray photoelectron spectroscopy (XPS) was performed using a Kratos Axis Ultra DLD system using a monochromatized Al Kα source ($h\nu$ = 1486.6 eV). A takeoff angle of 0° relative to the surface normal was used to sample the maximum surface depth. XPS peak fitting and analysis was performed with CasaXPS software. Energy calibration was referenced to the C 1s peak at 284.8 eV. Secondary electron microscopy (SEM) was performed using a FEI Quanta 200 FEG SEM. X-ray diffraction (XRD) was performed with a Rigaku Smartlab X-ray diffractometer in the 2-theta mode at a grazing angle of 0.5°. Synchrotron X-ray diffraction experiments were done at beamline 12.3.2 of the Advanced Light Source at Lawrence Berkeley National Laboratory. A monochromatic 10 keV X-ray beam was focused on the thin film sample placed in reflection mode into the beam. A Pilatus 1 M area detector was placed at 350 mm to record Debye rings diffracted by the sample. Alumina was used to determine the beam center and the sample to detector distance. The analysis was carried out at room temperature.

Determination of Electrochemically Active Surface Area (EASA). Electrochemically active surface areas of the different catalyst surfaces relative to the flat polycrystalline copper foil control were measured via a procedure described by Kanan and co-workers with some modifications.[12−14] The same electrochemical cell as the one used for the CO2R study was employed. A Nafion proton exchange membrane was used to separate the cathode and anode chambers, and 0.1 M $HClO_4$ was used as the electrolyte. Cyclic voltammetry was carried out in a potential range where faradaic processes are absent (−0.15 to −0.25 V vs Ag/AgCl) and at six different scan rates (100, 80, 60, 40, 20, and 10 mV s^{-1}). The geometric current density was then plotted as a function of scan rate; the slope of this curve is equal to the double layer capacitance (Figure S6). Since this double layer capacitance is directly proportional to the surface area, roughness factors relative to flat and polycrystalline copper can be determined.

Preparation of Electrolytes. 0.1 M $CsHCO_3$ electrolyte was prepared by saturating 0.05 M Cs_2CO_3 with CO_2 until the pH was 6.8. 0.1 M $KHCO_3$ electrolyte was prepared in a similar way. All electrolytes were prepared using 18.2 MΩ DI water from a Millipore system. No pre-electrolysis or other pretreatment of the electrolyte was carried out before CO2R.

Electrochemical Measurements. Electrochemical measurements were controlled by a Biologic SP-300 potentiostat. Ambient pressure CO2R was carried out in a custom-made gastight electrochemical cell made of PEEK and fitted with rubber o-rings.[34] The configuration of the electrochemical cell is such that the working electrode sits parallel with respect to the counter electrode (platinum foil) to ensure a uniform potential distribution across the surface. The geometric surface area of both electrodes was 1 cm^2. A custom glass frit fabricated by Adams & Chittenden Scientific Glass was used to saturate the electrolyte with CO_2 as well as to provide solution convection.[28] A Selemion AMV anion exchange membrane was used to separate the anode and cathode chambers. Each of these chambers in this cell contains a small volume of electrolyte (1.8 mL each) to concentrate liquid products and therefore increase detection limits. Before electrochemical testing, the electrochemical cell was sonicated in 20 wt % nitric acid solution for 1 h.

Before carrying out CO2R, the electrolyte in the cathode chamber was purged with CO_2 for at least 15 min. During electrolysis, CO_2 was constantly bubbled through the electrolyte at a flow rate of 5 sccm to prevent depletion of CO_2 in the electrolyte and to allow continuous analysis of gaseous products via a gas chromatograph. The flow rate of CO_2 was controlled with a mass flow controller (Alicat Scientific), and the gas was first humidified with water by passing it through a bubbler to minimize evaporation of electrolyte. For all experiments, platinum foil was used as the counter electrode and Ag/AgCl electrode (leak free series) from Innovative Instruments, Inc., was used as the reference. Applied potentials were converted to the RHE reference scale using the equation

$$E(\text{vs RHE}) = E(\text{vs Ag/AgCl}) + 0.197\ \text{V} + 0.0591\ \text{pH}$$

where the pH was 6.8. To ensure the accuracy of the reference electrodes, a calibration was performed with a homemade reversible hydrogen electrode. Before bulk electrolysis was carried out, the solution resistance was determined using potentiostatic electrochemical impedance spectroscopy by

DOI: 10.1021/acs.jpcc.7b03673
J. Phys. Chem. C 2017, 121, 14191−14203

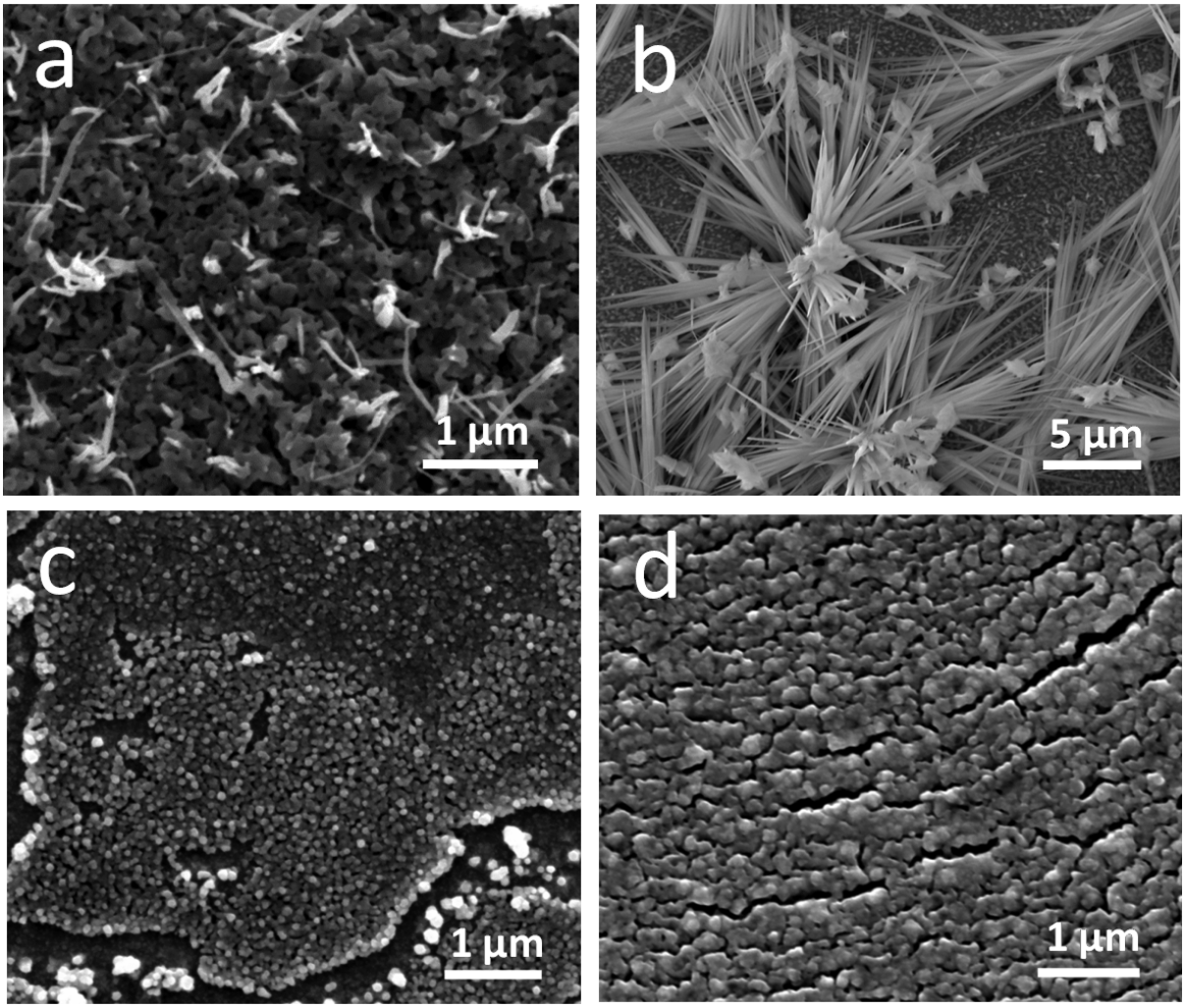

Figure 1. SEM images of oxide-derived catalysts after reduction: (a) OD Cu; (b) OD NWs 150s; (c) EC Cu; and (d) EOD Cu 100s. Note the larger scale bar for OD NWs.

scanning through a frequency range of 1 MHz to 10 Hz. The potentiostat software was then set to compensate for 85% of the measured solution resistance.

Product Analysis. For gas product analysis, a gas chromatograph (MG#3 SRI Instruments) equipped with a packed 12 in. long HaySep D column was used. For detection of gas products, a flame ionization detector (FID) with a methanizer was used to detect hydrocarbons (CO, CH_4, C_2H_4, and C_2H_6) with argon as the carrier gas. A thermal conductivity detector (TCD) was used to detect hydrogen with argon as the carrier gas. Calibration of the gas chromatograph was done using custom calibration gas tanks from Airgas each containing varying amounts of hydrogen, carbon monoxide, methane, ethylene, and ethane. After passing through the cell, the CO_2 was allowed to flow directly into the gas sampling loop of the GC for online gaseous product analysis, which was carried out every 15 min. For all experiments, electrolysis was allowed to proceed for 70 min with gas analysis done at 10, 25, 40, 55, and 70 min. Values were averaged to yield the data reported.

The liquid products were collected from the cathode and anode chambers after electrolysis and analyzed by high-performance liquid chromatography (HPLC) on an UltiMate 3000 instrument from Thermo Scientific. Vials with the collected samples were placed in an autosampler holder, and 10 μL of sample was injected into the column. The column used was an Aminex HPX 87-H (Bio-Rad), and diluted sulfuric acid (1 mM) was used as the eluent. The temperature of the column was maintained at 60 °C in a column oven, and the separated compounds were detected with a refractive index detector (RID). Calibrations were performed using dilute solutions of the expected products of the CO_2 reduction reaction (CO2R): glyoxal, glycolaldehyde, formate, formaldehyde, acetate, ethylene glycol, hydroxyacetone, acetaldehyde, methanol, allyl alcohol, ethanol, propionaldehyde, and *n*-propanol.

Investigation of the Effects of CO_2 Partial Pressure. To study the effects of reduced CO_2 partial pressures on the selectivity and current density of Cu foil, three different mixtures of Ar and CO_2 were used (0.6, 0.8, and 1.0 atm of CO_2). For example, to obtain 0.6 atm of CO_2, a flow rate of 3 sccm of CO_2 and 2 sccm of Ar was selected and used to saturate the 0.1 M $CsHCO_3$ electrolyte in the electrochemical cell for at least 15 min. Besides changing the purge gas, all other experimental procedures were identical to those described above.

Modeling Information. The modeling approach, which is based on adapting the 1D reaction-diffusion model of Gupta et al.,[35] is described in detail in the Supporting Information.

DOI: 10.1021/acs.jpcc.7b03673
J. Phys. Chem. C 2017, 121, 14191−14203

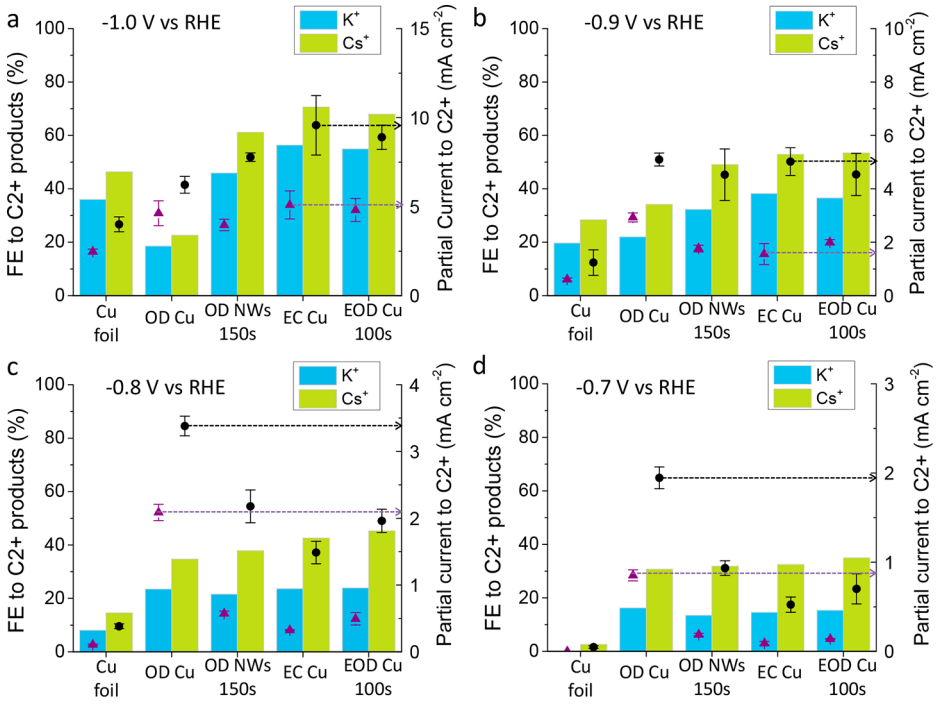

Figure 2. Faradaic efficiencies and partial current densities toward C_{2+} products for catalysts tested in both K^+ electrolyte and Cs^+ electrolyte: (a) −1.0 V vs RHE; (b) −0.9 V vs RHE; (c) −0.8 V vs RHE; (d) −0.7 V vs RHE. Purple triangles and black circles correspond to partial current density values to C_{2+} products for samples tested in K^+ electrolyte and Cs^+ electrolyte, respectively. Bar graphs correspond to faradaic efficiency values (blue, K^+ electrolyte; green, Cs^+ electrolyte). More detailed faradaic efficiency and current density data are available in the Supporting Information.

RESULTS AND DISCUSSION

Structural Characterization. SEM images of each of the four oxide-derived copper catalysts (OD Cu, OD NWs, EC Cu, and EOD Cu) in their reduced state are shown in Figure 1. For OD NWs, the length and density of the nanowire array can be tuned by varying the length of the chemical treatment step. The OD NWs shown in Figure 1 were treated for 150 s and will be referred to as OD NWs 150s. Similarly, the thickness of the oxide layer for EOD Cu can be adjusted by changing the electrodeposition time. The EOD Cu shown in Figure 1 was prepared by electrodepositing Cu_2O for 100 s and will be referred to as EOD Cu 100s. Additional SEM and optical images of the catalysts are shown in the Supporting Information (Figures S7−S13). Included in these figures are the SEM images of EOD Cu deposited for different times (50s, 200s, and 300s) as well as OD NWs treated for different times (75s, 300s, and 600s).

Oxide-derived nanocrystalline copper (OD Cu), Figure 1a, consists of a porous and aggregated structure made up of nanocrystalline copper grains with nanowire-like appendages protruding from the surface. Oxide-derived Cu nanowires (OD NWs 150s), Figure 1b, present a morphology consisting of long and dense nanowires emanating from nucleation sites on the surface. Electrochemically cycled copper (EC Cu), Figure 1c, consists of large islands of agglomerated round nanoparticles which are interconnected and appear nanocrystalline. Reduced electrochemically deposited copper oxide (EOD Cu 100s), Figure 1d, also consists of agglomerated round nanoparticles, and the morphology appears to be the most uniform compared to the other catalysts. Synchrotron X-ray diffraction was used to determine the crystallographic orientation of these different oxide-derived Cu catalysts. The XRD patterns show that all of the samples are highly polycrystalline with no specific preference for any orientation.

The electrochemically active surface area (EASA) of the catalysts (including OD NWs of varying density and EOD Cu of varying thickness) was also determined through cyclic voltammetry by measurement of the double layer capacitance. The roughness factor (RF) was normalized to polycrystalline copper, and the results are shown in Figure S6 and Table S2. OD Cu has the highest RF of 103, followed by EOD Cu 100s at 17.0, OD NWs 150s at 9.95, and EC Cu at 6.20.

Overview of CO_2 Reduction Measurements. The activity of the catalysts (including Cu foil as control) were tested in 0.1 M $KHCO_3$ (K^+ electrolyte) and 0.1 M $CsHCO_3$ (Cs^+ electrolyte). Previous reports have shown that optimal C−C coupling activity occurs in the range from ∼ −0.7 to −1.0 V vs RHE, and we therefore chose to test the catalysts in this applied voltage range.[9,15,16,20,36] All catalysts were tested for 70 min at −0.7, −0.8, −0.9, and −1.0 V vs RHE. For each catalyst, cation, and applied voltage condition, the analysis was performed three times to ensure the reproducibility and fidelity of the data. Thus, the experimental evaluation of CO_2 electroreduction activity in this portion of the study comprises the results of 168 individual experiments: 4 OD Cu catalyst configurations and the Cu foil control, 4 values of the applied potential, and 2 electrolyte conditions, and 3 repeats. Tables containing the detailed CO2R results are presented in the Supporting Information: Table S4, summary of C_2 product generation for all catalysts; Tables S19−S34, current density and FE for major products; Tables S35−S50, FE for minor products. All of the current density and faradaic efficiency data in this study are reported as the mean with the standard deviation as the uncertainty.

Role of Electrolyte Cation on C−C Coupling. For EOD Cu and OD NWs, the processing conditions allow for some

DOI: 10.1021/acs.jpcc.7b03673
J. Phys. Chem. C 2017, 121, 14191−14203

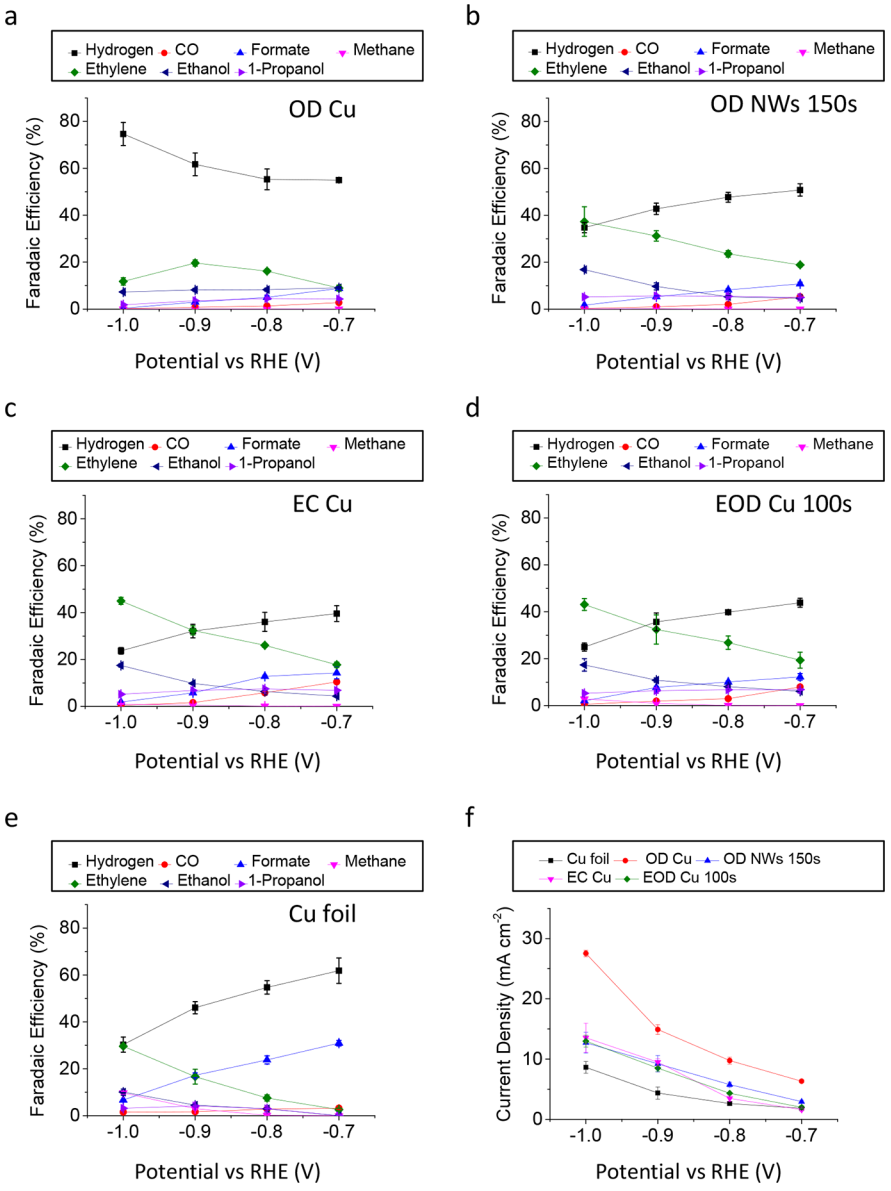

Figure 3. Faradaic efficiencies of major CO2R products from −0.7 to −1.0 V vs RHE in 0.1 M $CsHCO_3$ for (a) OD Cu, (b) OD NWs 150s, (c) EC Cu, (d) EOD Cu 100s, and (e) Cu foil. Current densities from −0.7 to −1.0 V vs RHE for each catalyst are shown in part f. More detailed faradaic efficiency and current density data are available in the Supporting Information.

control over the morphology. We used the conditions which produced the highest C_{2+} selectivity (EOD 100s and OD NWs 150s) for the comparison with the other two preparations. Figure 2 summarizes the C_{2+} selectivity of the four oxide-derived Cu catalysts at each of the applied potentials in both the K^+ electrolyte and Cs^+ electrolyte (solid blue and green bars). Current density is shown by points referenced to the right-hand axis. For reference to earlier studies of oxide-derived Cu, Table S3 presents a comparison of the C_{2+} product selectivity measured in this study using the K^+ electrolyte with values reported in the literature reports using the same class of catalyst. In all cases, the agreement is very good.

The most striking observation in Figure 2 is that, for all of the catalysts (including Cu foil), higher selectivity and partial current densities toward C_{2+} products can be attained using a Cs^+ electrolyte compared to a K^+ electrolyte at all applied potentials. Also, it appears that the selectivity to C_{2+} products for most of the catalysts peaks at −1.0 V vs RHE regardless of the cation used, which is in agreement with previous reports.[9,15,16] The increase in C_{2+} selectivity for Cu foil with the larger cation is also consistent with prior reports;[29,31] it is interesting that increases are also seen for the nanostructured Cu electrocatalysts. Focusing on Figure 2a, which contains the data for a bias of −1.0 vs RHE, the C_{2+} product selectivity is highest for EC Cu at 70.6% (±2.24), followed by EOD Cu 100s at 68.5% (±5.00), OD NWs at 61.1% (±6.18), Cu foil at 46.4% (±1.18), and finally OD Cu at only 22.6% (±1.50).

Regardless of the cation used, nearly all variants of oxide-derived catalysts perform better at all potentials than the Cu foil control sample, which is also consistent with previous studies of oxide-derived copper.[12,15,16,18,22] The exception is OD Cu operated at −1.0 V, which has a lower selectivity; we believe this is due to mass transport limitations due to its inherent high surface area, which will be discussed in more detail below. Again, with the exception of OD Cu, the selectivity toward C_{2+} products decreases at less negative applied potentials. At −0.9

DOI: 10.1021/acs.jpcc.7b03673
J. Phys. Chem. C 2017, 121, 14191−14203

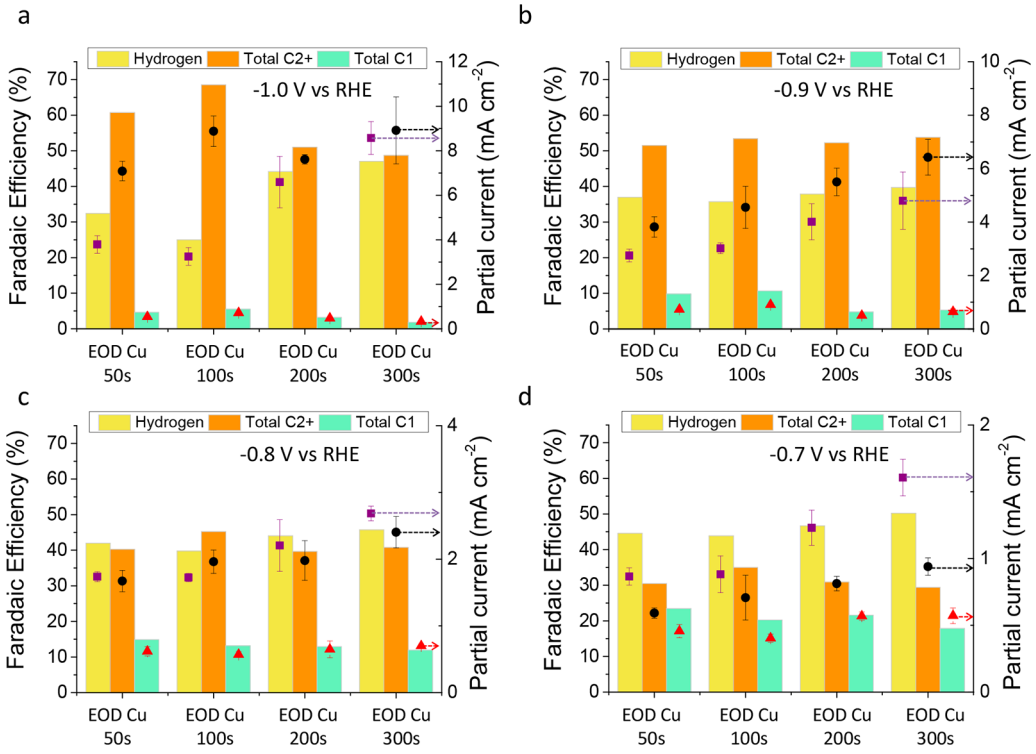

Figure 4. Faradaic efficiencies and partial current densities toward H_2, C_{2+} products and C_1 products for different thicknesses of electrodeposited Cu oxide layer tested in Cs^+ electrolyte at different applied potentials: (a) −1.0 V vs RHE; (b) −0.9 V vs RHE; (c) −0.8 V vs RHE; (d) −0.7 V vs RHE. Purple squares, black circles, and red triangles correspond to H_2, C_{2+} and C_1 partial current density values, respectively. Bar graphs correspond to faradaic efficiency values of H_2 (yellow), C_{2+} products (orange) and C_1 products (green). More detailed faradaic efficiency and current density data are available in the Supporting Information.

and −0.8 V vs RHE, EC Cu and EOD Cu 100s remain the best performers and boast a C_{2+} selectivity of >50 and >40% at these two potentials. At the lowest tested overpotential of −0.7 V vs RHE, the C_{2+} selectivity in Cs^+ electrolyte of all the oxide-derived catalysts remains relatively high, >30%. This contrasts with copper foil which has a very low FE for C_{2+} products in Cs^+ electrolyte and appears not to yield any C_{2+} products in K+. Intriguingly, at −0.7 V vs RHE, the C_{2+} selectivity for all of the oxide-derived catalysts seems to converge at ∼30% in Cs^+ electrolyte and ∼15% in K^+ electrolyte.

Another benefit of enhancing the selectivity toward C_{2+} products is the suppression of C_1 products. Figure S14 summarizes the selectivity for C_1 production as a function of bias for both K^+ and Cs^+ electrolyte. From −0.7 to −1.0 V, use of Cs^+ appears to suppress the formation of C_1 products such as CO, $HCOO^-$, and CH_4. At a potential of −1.0 V on EC Cu, for example, only 3.25% selectivity toward C_1 products was observed with Cs^+ electrolyte compared to 12.0% with K^+ electrolyte at the same potential. Similar trends were observed for all other oxide-derived catalysts. The most pronounced suppression of C_1 products was observed with OD Cu at −1.0 V in Cs^+ electrolyte, as only 0.46% selectivity to C_1 products was observed. In this case, methane was not even observed as a product (Table S19).

Product Distribution with Cs^+ Electrolyte. Next, we look in detail at the product distributions as a function of applied potential with Cs^+ electrolyte for the different oxide-derived catalysts, as shown in Figure 3. At a potential of −1.0 V, EC Cu exhibits the lowest selectivity to hydrogen evolution at 23.7%, followed by EOD Cu 100s at 25.0%, OD NWs 150s at 34.8%, Cu foil at 30.3%, and finally OD Cu at 74.6%. The selectivity to hydrogen increases at decreased overpotentials (OD Cu is an exception), which follows the trend of the Cu foil control, Figure 3e. A characteristic of oxide-derived catalysts is the suppression of the reaction pathway toward methane compared to Cu foil; this effect is more pronounced with the use of a Cs^+ electrolyte. For example, at −1.0 V vs RHE, Cu foil exhibits a selectivity of 9.74% toward methane, whereas this value is <3% for all variants of oxide-derived copper. Looking at the distribution of C_{2+} products, it appears that ethylene and ethanol are the most dominant. For example, EC Cu has a selectivity of 45.0 and 17.5% for ethylene and ethanol, respectively, at −1.0 V. For the same catalyst and potential, only 0.93% selectivity toward methane was observed.

For all catalysts and potentials, it appears that, whenever high ethylene selectivity is observed, high ethanol selectivity is observed as well. This is consistent with measurements made by Jaramillo and co-workers on Cu foil,[9] which suggest that C_2 products follow similar initial reaction pathways, although it is not yet entirely clear what determines their branching ratios.[37] We further note that our use of an electrochemical cell with small electrolyte volume allows complete accounting for all minor products, most of which are in the liquid phase (Tables S35−S50). Intriguingly, the selectivity toward minor products such as 1-propanol, allyl alcohol, and propionaldehyde seems to be lowest at −1.0 V. The maximum selectivity for these products occurs at less negative applied potentials, −0.9 or −0.8 V (depending on catalyst), which is qualitatively consistent with results from Jaramillo and co-workers on Cu foil in 0.1 M $KHCO_3$.[9] For example, with EC Cu at −0.7 V, the selectivity to 1-propanol is 6.87%, which makes up 21.2% of the total C_{2+} being produced. On the other hand at −1.0 V, 1-

DOI: 10.1021/acs.jpcc.7b03673
J. Phys. Chem. C 2017, 121, 14191−14203

propanol only makes up 7.37% of the total C_{2+} composition. Ethylene and ethanol make up 88.5% of total C_{2+} products at −1.0 V; this suggests that at higher overpotentials C−C coupling reaction pathways favor ethylene and ethanol over other minor products.

Finally, the composition of the C_{2+} products as a function of potential for all catalysts in Cs^+ electrolyte and K^+ electrolyte was also determined (Table S4). It appears that changing the cation enhances all C−C coupled products equally, with no significant change of the C_{2+} product composition. This suggests that the larger Cs^+ cation enhances the initial C−C coupling step (which explains the suppression of methane) but has little effect on the subsequent steps of the reaction pathways.

Comparison of Oxide-Derived Catalyst Activity for CO2R. The careful benchmarking of the CO2R activity of the oxide-derived Cu catalysts not only allows a quantitative comparison of their activities but also enables insight into how they produce enhanced C_{2+} product yields. A number of factors including surface facet orientation and grain boundaries are believed to affect the selectivity of copper catalysts toward C_{2+} products. For example, the Cu(100) surface has been shown to have particularly high selectivity toward ethylene, whereas the Cu(111) surface has been shown to favor methane formation.[6,38] Kanan and co-workers have shown that grain boundaries are highly active sites for C−C coupling and removal of these sites results in loss of selectivity toward C_{2+} products.[39] Also, work by Yeo and co-workers has shown that having a smaller crystallite size and therefore more grain boundaries appears to increase the selectivity toward ethylene.[40] Indeed, from the SEM images, it appears that the samples are mostly composed of nanocrystalline, agglomerated particles, suggesting a higher density of grain boundaries compared to polycrystalline copper.

The high density of grain boundaries and absence of a preferred orientation would lead to a prediction of similar selectivity toward C_{2+} products for the catalysts compared in this study. Indeed, the selectivity toward C_{2+} products is very similar at the lowest applied potential of −0.7 V. However, at higher overpotentials, the selectivity of the catalysts diverges. Notably, OD Cu produces mostly hydrogen at −1.0 V vs RHE, while the other catalysts produce >60% C_{2+} products. We hypothesized that the reason for this difference is that, at very negative applied potentials, higher surface area leads to a mass transfer bottleneck for the CO_2 reactant. However, at less negative applied potentials, the current density is much lower and thus depletion of CO_2 and the associated concentration polarization effects at the catalyst surface are less severe.[41] To test this hypothesis, we performed a series of experiments using morphology tuning afforded by the EOD Cu synthesis method.

Role of Surface Area. EOD Cu samples were made with different electrodeposition times: EOD Cu 50s, EOD Cu 200s, and EOD Cu 300s, with a longer deposition time leading to a thicker Cu_2O layer (SEM images in Figure S12). After reduction to the metallic state, the roughness factor (RF) was measured (Figure S6). As expected, increasing the electrodeposition time for EOD Cu increases the RF. A range of about a factor of 2 was obtained: 12.8, 17.0, 20.9, and 24.0 for 50s, 100s, 200s, and 300s, respectively (Table S2). The H_2, C_{2+}, and C_1 FEs and current densities obtained in Cs^+ electrolyte for this set of samples are shown in Figure 4.

For the smaller overpotentials, the EOD Cu electrocatalysts have similar product distributions, independent of their roughness factor. However, at the most negative applied potential of −1.0 V, where the current density and consumption of CO_2 are the highest, it is apparent that there is an optimum RF where selectivity and partial current density to C_{2+} products is highest, which corresponds to that of EOD Cu 100s. On the other hand, at this same potential at −1.0 V, selectivity and partial current density toward C_1 products decrease with increasing RF (Figure 4). These trends seem to be consistent with results from Yeo and co-workers in K^+ electrolyte, where they also observed an optimal RF for enhancing C_{2+} products and suppressing hydrogen as well as a decrease in C_1 products with increasing RF.[16] At lower potentials, the C_{2+} selectivity for all samples appears to be similar, although the partial current density increases with higher RF samples due to their higher surface area (roughness factor). Interestingly, in going from −1.0 to −0.9 V, the selectivity to hydrogen for the higher RF samples (200s and 300s) actually decreases, which is opposite to what was observed for the thinner samples (50s and 100s).

To further investigate the effect of surface area/RF on the selectivity of oxide-derived catalysts, we also synthesized OD NWs of varying nanowire lengths and densities (Figure S9) by varying the treatment time (75s, 300s, and 600s) and we observed similar trends (Figure S15) to what was observed with EOD Cu. RF values for these OD NWs samples are also shown in Table S2.

Relationship between Selectivity, CO_2 Mass Transport, and Local pH. A consistent explanation of the observation of an optimal RF for maximizing C−C coupling (within a given synthesis scheme) can be provided by considering the competing effects of local pH and CO_2 concentration. CO_2 reduction consumes hydrogen atoms from water and releases hydroxide anions, leading to an increase in the pH near the cathode surface. The higher geometrical current densities for the high surface area catalysts magnify this effect.[15,16,19,42]

The effect of pH on the product distribution for both CO_2 and CO reduction on Cu electrodes has been studied experimentally. Koper and co-workers[43,44] and Nilsson and co-workers[22] have shown that, at high pH, C−C coupling of CO occurs at lower overpotentials on the RHE scale than at low pH. In this case, both sets of investigators demonstrate that ethylene formation occurs at lower onset potentials on the RHE scale in more basic (pH 13) as compared to neutral (pH 7) conditions. These observations are relevant because the reduction of CO_2 to ethylene proceeds via the formation of CO. It is also notable that if the experimental results are represented on the SHE scale there is no effect of pH, indicating that the C−C bond formation does not involve change transfer.[45] Recent theoretical work by Goddard and co-workers also suggests that, at high pH, pathways to CH_4 are blocked kinetically and are therefore suppressed.[46] C−C bond formation is unaffected by pH, and consequently, the kinetically dominant pathway at high pH is CO−CO coupling, the first step along the path to ethylene.[46]

During CO2R, depending on the catalyst morphology, mass transfer conditions, and buffering capacity of the electrolyte, the surface pH can rise above the bulk pH, as has been shown previously by simulation.[35,41] Indeed, this rise in surface pH has been proposed to be the reason for high C_{2+} product selectivity on high surface area copper electrodes.[15,16,19,47] However, the OH^- anions that are generated can concurrently react with CO_2 to form HCO_3^- and CO_3^{2-} anion and thereby reduce the

DOI: 10.1021/acs.jpcc.7b03673
J. Phys. Chem. C 2017, 121, 14191−14203

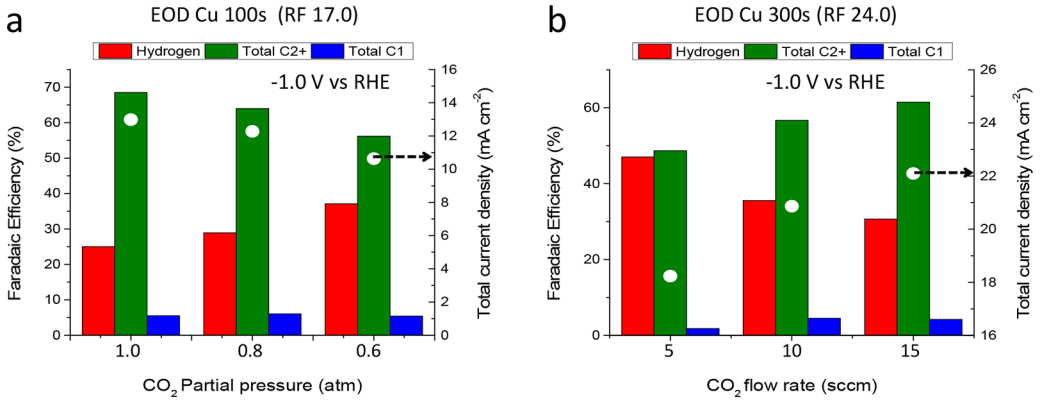

Figure 5. Faradaic efficiencies and partial current densities toward H_2, C_{2+} products and C_1 products at −1.0 V vs RHE for (a) EOD Cu 100s with different CO_2 partial pressures and (b) EOD Cu 300s with different flow rates of CO_2. A lower CO_2 partial pressure results in a lower concentration of dissolved CO_2, while a higher flow rate results in a smaller mass-transfer boundary layer thickness. White circles correspond to total current density values. Bar graphs correspond to faradaic efficiency values. More detailed faradaic efficiency and current density data are available in the Supporting Information (Tables S5 and S6).

CO_2 concentration at the cathode.[3,35,41] Therefore, if the pH at the cathode surface is too large, the concentration of CO_2 at the cathode is lowered, which leads to an inhibition in the rate of CO2R. We note here that the approach to equilibrium is highly dependent on the kinetics of the reaction of CO_2 and OH^- anions to form HCO_3^- and CO_3^{2-} anions.

The trade-off between increasing surface pH, which can contribute to the net enhancement in the rate of C−C coupling and decreasing CO_2 concentration suggests that there should be an optimal value of the RF for the oxide-derived catalysts to perform optimally. If the RF is too high, then the electroactive surfaces will be in an environment where dissolved CO_2 is depleted and H_2O is the only available reactant. This scenario appears to be occurring on OD Cu (RF = 103, Table S2) as hydrogen evolution dominates its activity at −1.0 V vs RHE (Figure 3a). Also, in contrast to the other electrocatalysts, hydrogen selectivity decreases with more positive applied overpotential; this is due to the reduction in current density (see Figure 3f), which in turn reduces the deleterious effect of CO_2 mass transport limitations. We propose that this is the reason that similar product selectivity is exhibited by all oxide-derived samples at −0.7 V (Figure 1), where mass transport limitations are expected to have a less significant effect. Similarly, we observe this effect to a less significant degree for EOD Cu 200s and EOD Cu 300s, which have RF values of 20.9 and 24.0, respectively. The optimum RF value would therefore be able to induce a high local pH but not so high as to lead to CO_2 mass transport limitations.

As a result of this analysis, we hypothesized that, for catalysts with optimum RF values, reducing the CO_2 concentration should reduce the selectivity toward C_{2+} products and increase the hydrogen selectivity. On the other hand, increasing the CO_2 supply for catalysts with high RF values would be expected to improve selectivity toward C_{2+} products and decrease the hydrogen selectivity. To investigate the first idea, we tested EOD Cu 100s at −1.0 V vs RHE at lower partial pressures of CO_2, 0.8 and 0.6 atm, balanced to 1 atm with Ar. As shown in Figure 5, lowering the CO_2 partial pressure from 1.0 to 0.6 atm does indeed result in a decrease in C_{2+} selectivity from 68.5 to 56.2%. Furthermore, the hydrogen selectivity increases from 25.0 to 37.1%.

To increase the CO_2 supply for high RF catalysts, the thickness of the mass-transfer boundary layer can be reduced by increasing the CO_2 flow rate convection to the electrochemical cell. The decrease in the mass-transfer boundary layer thickness with increasing CO_2 flow rate was verified experimentally (see Table S7). The performance of EOD Cu 300s was measured at flow rates of 10 and 15 sccm for a potential of −1.0 V vs RHE (all experiments reported thus far were carried out at a flow rate of 5 sccm). As shown in Figure 5b, decreasing the mass-transfer boundary layer thickness causes the C_{2+} selectivity to increase from 48.7% at 5 sccm to 61.4% at 15 sccm. At the same time, the hydrogen selectivity decreases from 47.0% at 5 sccm to 30.7% at 15 sccm. We also investigated EOD Cu 100s at higher CO_2 flow rates of 10 and 15 sccm; the results are shown in Figure S16 and Table S8. The current density and hydrogen selectivity were not affected by increasing the flow rate because the catalyst was not limited by the availability of CO_2 at 5 sccm. However, at the higher flow rates, a small increase in C_1 selectivity and a small decrease in C_2 selectivity were observed, which we attribute to the decreased mass-transfer boundary layer thickness somewhat mitigating the rise in the local pH. As discussed above, theoretical studies suggest that the increase in pH will suppress the formation of CH_4 relative to C_{2+} products.[46]

Numerical Modeling of Oxide-Derived Catalysts. The explanations for our experimental observations have been based on the competition between the local pH rise which aids C−C coupling and depletion of CO_2 which can reduce C_{2+} selectivity. To gain a deeper insight into these effects, we calculated the average surface pH as well as the average CO_2 concentration at the surface of the catalysts using an approach similar to that described by Gupta et al.[35]

In this model, the catalyst is assumed to be flat regardless of its true morphology. The experimental rate of CO_2 consumption and OH^- generation for each oxide-derived catalyst at each potential can be calculated on the basis of the geometric current density and product distribution (Table S11). This information is used as an input to the model. The kinetics of the reaction of OH^- with CO_2 or with bicarbonate anions are described by the forward and reverse rate coefficients for these reactions (see Table S9). The mass-transfer boundary layer thickness used in the model was determined experimentally by measuring the limiting current density of the reduction of $Fe(CN)_4^{3-}$ under identical hydrodynamic conditions (see Table S7).

DOI: 10.1021/acs.jpcc.7b03673
J. Phys. Chem. C 2017, 121, 14191−14203

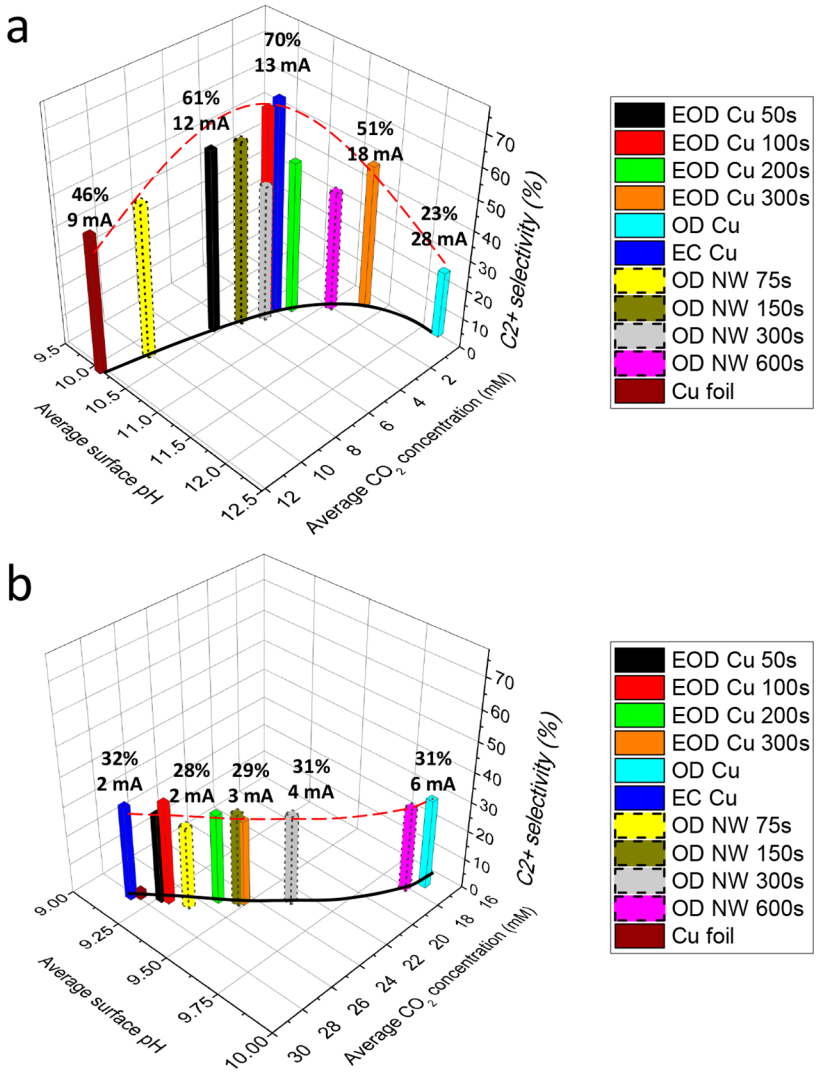

Figure 6. Numerical simulation results of the average CO_2 concentration and average surface pH of the various oxide derived catalysts for (a) oxide-derived catalysts at −1.0 V vs RHE and (b) oxide-derived catalysts at −0.7 V vs RHE. Average surface pH and average CO_2 concentrations are represented on the horizontal axes. C_{2+} selectivity is represented on the vertical axis. The bars representing the OD NW system have dashed borders. The relationship between CO_2 concentration and pH is represented by the black curve and the red dashed curve is a guide to the eye representing the C_{2+} selectivity of the various catalysts. The C_{2+} selectivity as well as the current density (given in mA per 1 cm^2 geometric area) is given at selected locations. Detailed modeling results are available in the Supporting Information (Tables S12 and S13).

The average surface CO_2 concentration and average surface pH were calculated for OD Cu, EC Cu, OD NWs (75s to 600s), and EOD Cu (50s to 300s) at −1.0 and −0.7 V vs RHE (from Figure 2), and the results together with their respective experimental C_{2+} selectivity are shown in Figure 6. For all cases, the experimentally determined geometric current densities and the respective product distribution were used to calculate the CO_2 consumption rate and OH^- generation rate as inputs to the model.

The solid black curve in Figure 6a illustrates the calculated relationship between the average CO_2 concentration and the pH near the cathode surface (a discussion of the origin of this curve is shown in the Supporting Information). The variation in the current density is also shown for selected locations on this curve, with the surface pH increasing and CO_2 concentration decreasing with increasing current density. The height of the bars gives the C_{2+} product selectivity, and the red dashed curve, drawn as a guide for the eye, represents the variation in C_{2+} product selectivity as a function of the cathode surface pH and CO_2 concentration. For an applied voltage of −1 V vs RHE, a maximum in the C_{2+} product selectivity is observed for a pH of ∼10.6 and a CO_2 surface concentration of ∼4.1 mM, corresponding to a current density of ∼13.3 mA/cm^2. Catalysts having a high surface pH have lower average CO_2 concentrations, corresponding to high current densities, and vice versa. Catalysts lying on the right side of the curve experience CO_2 depletion (EOD Cu 300s, OD NWs 600s, and OD Cu) and have low C_{2+} selectivities. For example, OD Cu, which has the highest RF of 103 is completely depleted of CO_2 at −1.0 V vs RHE, which explains why it has the highest hydrogen selectivity of 74.6% as well as the lowest C_{2+} selectivity of 22.6%. Similarly, EOD Cu 300s and OD NWs 600s have low C_{2+} selectivities (48.7 and 40.8%, respectively) and high hydrogen selectivities (47.0 and 55.8%, respectively). The catalysts with the highest C_{2+} selectivity (EC Cu and EOD Cu 100s) appear in the middle of this curve, and are characterized by similar average pH (∼10.6), average CO_2 concentration (∼4.09 mM), and C_{2+} selectivity (∼69%). These

DOI: 10.1021/acs.jpcc.7b03673
J. Phys. Chem. C 2017, 121, 14191−14203

catalysts have an optimum RF for their morphology, leading to a higher pH and thus more C−C coupling relative to the formation of CH_4 but not so high as to result in a significant depletion of CO_2 near the cathode. The left side of the curve represents catalysts which have lower RF values, resulting in a lower pH rise and therefore lower selectivity toward C_{2+} products.

A similar set of results are shown in Figure 6b for an applied voltage of −0.7 V vs RHE. Notice that, in this case, the variations in the pH and CO_2 concentration near the catalyst surface differ less significantly from those in the bulk electrolyte (pH = 6.8 and CO_2 concentration = 33 mM) due to the lower current densities observed at this applied potential. Furthermore, none of the catalysts appear to experience CO_2 depletion conditions and differences in pH between all of the catalysts are less drastic, as are also the current densities. This would explain why the C_{2+} selectivity for all catalysts converges to a very similar value of ∼30%. Only Cu foil is an outlier, exhibiting the lowest C_{2+} selectivity, and this is likely due to a lower concentration of grain boundaries (active sites for C−C coupling) relative to what occurs for the OD Cu catalysts.[14,39,40]

Finally, on the basis of the modeling results, we hypothesized that application of a more negative potential would result in current densities exceeding the optimal value of ∼12−14 mA cm^{-2}, leading to CO_2 depletion effects. To test this hypothesis, we conducted CO2R at −1.1 V vs RHE for OD Cu, OD NWs 150s, EC Cu, EOD Cu 100s, and Cu foil (Figure S19 and Table S18). The results show that CO_2 mass transport limitations occur for all oxide-derived catalysts. The previously optimally performing oxide-derived catalysts at −1.0 V vs RHE now only exhibit ∼35% C_{2+} selectivity, with ∼58% H_2 selectivity at −1.1 V vs RHE. Due to the large amount of current drawn by OD Cu at this potential (∼45 mA cm^{-2}), severe CO_2 depletion effects occur, resulting in predominantly H_2 production (91.7%) and only 5.4% selectivity toward C_{2+} products. It is interesting to note that, at −1.1 V vs RHE, Cu foil has its highest selectivity toward C_{2+} products (54.5%) and its lowest H_2 selectivity (29.6%). This is in agreement with the mass transport, as the current density drawn by Cu foil at this potential is 13.5 mA cm^{-2}, which is close to the optimum for generating C_{2+} products identified in Figure 6a.

In summary, we find that at low applied voltages (viz., −0.7 V vs RHE), where the effects of CO_2 mass transfer to the cathode are minimal, there is relatively little effect of pH and local CO_2 concentration on the selectivity to C_{2+} products. At high applied potential (viz., −1.0 V vs RHE), where the extent of mass transfer limitation becomes significant, we observe that there is an optimal range of pH and CO_2 concentration for achieving a high C_{2+} selectivity. In this range, the pH is elevated relative to that in the bulk electrolyte, but the rates of CO_2 conversion to HCO_3^- and CO_3^{2-} anions are not sufficiently high to draw down the CO_2 concentration to a point where it negatively affects the C_{2+} product selectivity. In this regime, the C_{2+} product selectivity may also be enhanced by the suppression of the kinetics to C_1 products at high pH.

CONCLUSIONS

The catalytic activities of four different variants of oxide-derived copper for electrochemical CO_2 reduction at −0.7 to −1.0 V vs RHE for two different cations in the electrolyte (Cs^+ and K^+) were compared. We find that use of the larger cation increases selectivity toward C_2 and C_3 (C_{2+}) products at all potentials for all catalysts including the Cu foil control. On the best performing oxide-derived catalyst, up to ∼70% selectivity toward C_{2+} products was observed with only ∼3% selectivity toward C_1 products at −1.0 V vs RHE. To our knowledge, this is the highest C_{2+} selectivity reported for CO_2 electroreduction in water under ambient conditions of 1 atm and room temperature. For the same conditions in K^+ electrolyte, the selectivity toward C_{2+} products was only 56%, which demonstrates the merits of combining a Cs^+ electrolyte with an oxide-derived catalyst. We also found that there is an optimum roughness factor for the oxide-derived layer to balance the benefits of having a high local pH but still maintaining a high concentration of the reactant species (dissolved CO_2). Finally, electrochemical transport modeling illustrates the relationship between catalyst roughness and CO_2 depletion and its effects on C_{2+} product selectivity. The present study shows that high C_{2+} product selectivity can be achieved by using a $CsHCO_3$ as the electrolyte together with oxide-derived Cu catalysts with a modest roughness factor.

ASSOCIATED CONTENT

Supporting Information

The Supporting Information is available free of charge on the ACS Publications website at DOI: 10.1021/acs.jpcc.7b03673.

Electrochemically active surface area measurements (EASA), secondary electron microscopy (SEM) images, X-ray photoelectron spectroscopy (XPS) measurements, X-ray diffraction (XRD) measurements, X-ray diffraction measurements, FE/current density data, modeling information and results and other experimental data (PDF)

AUTHOR INFORMATION

Corresponding Authors

*E-mail: alexbell@berkeley.edu.
*E-mail: jwager@lbl.gov.

ORCID

Alexis T. Bell: 0000-0002-5738-4645
Joel W. Ager: 0000-0001-9334-9751

Author Contributions

The manuscript was written through contributions of all authors. All authors have given approval to the final version of the manuscript.

Notes

The authors declare no competing financial interest.

ACKNOWLEDGMENTS

This material is based upon work performed by the Joint Center for Artificial Photosynthesis, a DOE Energy Innovation Hub, supported through the Office of Science of the U.S. Department of Energy under Award Number DE-SC0004993. Synchrotron X-ray diffraction measurements performed at Beamline 12.3.2 at the Advanced Light Source were supported by the Director, Office of Science, Office of Basic Energy Sciences of the U.S. Department of Energy under Contract No. DE-AC02-05CH11231. We thank the Molecular Graphics and Computation Facility, College of Chemistry, University of California Berkeley, supported by National Science Foundation grant CHE-080405, for providing access to computing resources. Y.L. acknowledges the support of an A*STAR National Science Scholarship.

DOI: 10.1021/acs.jpcc.7b03673
J. Phys. Chem. C 2017, 121, 14191−14203

REFERENCES

(1) Graves, C.; Ebbesen, S. D.; Mogensen, M.; Lackner, K. S. Sustainable Hydrocarbon Fuels by Recycling CO_2 and H_2O with Renewable or Nuclear Energy. *Renewable Sustainable Energy Rev.* **2011**, *15*, 1−23.

(2) Jones, J.-P.; Prakash, G. K. S.; Olah, G. A. Electrochemical CO_2 Reduction: Recent Advances and Current Trends. *Isr. J. Chem.* **2014**, *54*, 1451−1466.

(3) Hori, Y. Electrochemical CO2 Reduction on Metal Electrodes. In *Modern Aspects of Electrochemistry SE*; Vayenas, C., White, R., Gamboa-Aldeco, M., Eds.; Modern Aspects of Electrochemistry; Springer: New York, 2008; Vol. *42*, pp 89−189.

(4) Gattrell, M.; Gupta, N.; Co, A. A Review of the Aqueous Electrochemical Reduction of CO_2 to Hydrocarbons at Copper. *J. Electroanal. Chem.* **2006**, *594*, 1−19.

(5) Qiao, J.; Liu, Y.; Hong, F.; Zhang, J. A Review of Catalysts for the Electroreduction of Carbon Dioxide to Produce Low-Carbon Fuels. *Chem. Soc. Rev.* **2014**, *43*, 631−675.

(6) Hori, Y.; Takahashi, I.; Koga, O.; Hoshi, N. Electrochemical Reduction of Carbon Dioxide at Various Series of Copper Single Crystal Electrodes. *J. Mol. Catal. A: Chem.* **2003**, *199*, 39−47.

(7) Kuhl, K. P.; Hatsukade, T.; Cave, E. R.; Abram, D. N.; Kibsgaard, J.; Jaramillo, T. F. Electrocatalytic Conversion of Carbon Dioxide to Methane and Methanol on Transition Metal Surfaces. *J. Am. Chem. Soc.* **2014**, *136*, 14107−14113.

(8) Kim, D.; Resasco, J.; Yu, Y.; Asiri, A. M.; Yang, P. Synergistic Geometric and Electronic Effects for Electrochemical Reduction of Carbon Dioxide Using Gold-Copper Bimetallic Nanoparticles. *Nat. Commun.* **2014**, *5*, 4948.

(9) Kuhl, K. P.; Cave, E. R.; Abram, D. N.; Jaramillo, T. F. New Insights into the Electrochemical Reduction of Carbon Dioxide on Metallic Copper Surfaces. *Energy Environ. Sci.* **2012**, *5*, 7050−7059.

(10) Hori, Y.; Murata, A.; Takahashi, R. Formation of Hydrocarbons in the Electrochemical Reduction of Carbon Dioxide at a Copper Electrode in Aqueous Solution. *J. Chem. Soc., Faraday Trans. 1* **1989**, *85*, 2309.

(11) Singh, M. R.; Clark, E. L.; Bell, A. T. Thermodynamic and Achievable Efficiencies for Solar-Driven Electrochemical Reduction of Carbon Dioxide to Transportation Fuels. *Proc. Natl. Acad. Sci. U. S. A.* **2015**, *112*, E6111−E6118.

(12) Li, C. W.; Kanan, M. W. CO_2 Reduction at Low Overpotential on Cu Electrodes Resulting from the Reduction of Thick Cu_2O Films. *J. Am. Chem. Soc.* **2012**, *134*, 7231−7234.

(13) Verdaguer-Casadevall, A.; Li, C. W.; Johansson, T. P.; Scott, S. B.; McKeown, J. T.; Kumar, M.; Stephens, I. E. L.; Kanan, M. W.; Chorkendorff, I. Probing the Active Surface Sites for CO Reduction on Oxide-Derived Copper Electrocatalysts. *J. Am. Chem. Soc.* **2015**, *137*, 9808−9811.

(14) Li, C. W.; Ciston, J.; Kanan, M. W. Electroreduction of Carbon Monoxide to Liquid Fuel on Oxide-Derived Nanocrystalline Copper. *Nature* **2014**, *508*, 504−507.

(15) Ma, M.; Djanashvili, K.; Smith, W. A. Controllable Hydrocarbon Formation from the Electrochemical Reduction of CO_2 over Cu Nanowire Arrays. *Angew. Chem., Int. Ed.* **2016**, *55*, 6680−6684.

(16) Ren, D.; Deng, Y.; Handoko, A. D.; Chen, C. S.; Malkhandi, S.; Yeo, B. S. Selective Electrochemical Reduction of Carbon Dioxide to Ethylene and Ethanol on Copper(I) Oxide Catalysts. *ACS Catal.* **2015**, *5*, 2814−2821.

(17) Chen, C. S.; Handoko, A. D.; Wan, J. H.; Ma, L.; Ren, D.; Yeo, B. S. Stable and Selective Electrochemical Reduction of Carbon Dioxide to Ethylene on Copper Mesocrystals. *Catal. Sci. Technol.* **2015**, *5*, 161−168.

(18) Roberts, F. S.; Kuhl, K. P.; Nilsson, A. High Selectivity for Ethylene from Carbon Dioxide Reduction over Copper Nanocube Electrocatalysts. *Angew. Chem.* **2015**, *127*, 5268−5271.

(19) Kas, R.; Kortlever, R.; Milbrat, A.; Koper, M. T. M.; Mul, G.; Baltrusaitis, J. Electrochemical CO_2 Reduction on Cu_2O-Derived Copper Nanoparticles: Controlling the Catalytic Selectivity of Hydrocarbons. *Phys. Chem. Chem. Phys.* **2014**, *16*, 12194.

(20) Mistry, H.; Varela, A. S.; Bonifacio, C. S.; Zegkinoglou, I.; Sinev, I.; Choi, Y.-W.; Kisslinger, K.; Stach, E. A.; Yang, J. C.; Strasser, P.; et al. Highly Selective Plasma-Activated Copper Catalysts for Carbon Dioxide Reduction to Ethylene. *Nat. Commun.* **2016**, *7*, 12123.

(21) Raciti, D.; Livi, K. J.; Wang, C. Highly Dense Cu Nanowires for Low-Overpotential CO_2 Reduction. *Nano Lett.* **2015**, *15*, 6829−6835.

(22) Roberts, F. S.; Kuhl, K. P.; Nilsson, A. Electroreduction of Carbon Monoxide Over a Copper Nanocube Catalyst: Surface Structure and pH Dependence on Selectivity. *ChemCatChem* **2016**, *8*, 1119−1124.

(23) Chen, Y.; Li, C. W.; Kanan, M. W. Aqueous CO_2 Reduction at Very Low Overpotential on Oxide-Derived Au Nanoparticles. *J. Am. Chem. Soc.* **2012**, *134*, 19969−19972.

(24) Schreier, M.; Curvat, L.; Giordano, F.; Steier, L.; Abate, A.; Zakeeruddin, S. M.; Luo, J.; Mayer, M. T.; Grätzel, M. Efficient Photosynthesis of Carbon Monoxide from CO_2 Using Perovskite Photovoltaics. *Nat. Commun.* **2015**, *6*, 7326.

(25) Hsieh, Y.-C.; Senanayake, S. D.; Zhang, Y.; Xu, W.; Polyansky, D. E. Effect of Chloride Anions on the Synthesis and Enhanced Catalytic Activity of Silver Nanocoral Electrodes for CO_2 Electroreduction. *ACS Catal.* **2015**, *5*, 5349−5356.

(26) Koh, J. H.; Jeon, H. S.; Jee, M. S.; Nursanto, E. B.; Lee, H.; Hwang, Y. J.; Min, B. K. Oxygen Plasma Induced Hierarchically Structured Gold Electrocatalyst for Selective Reduction of Carbon Dioxide to Carbon Monoxide. *J. Phys. Chem. C* **2015**, *119*, 883−889.

(27) Jee, M. S.; Jeon, H. S.; Kim, C.; Lee, H.; Koh, J. H.; Cho, J.; Min, B. K.; Hwang, Y. J. Enhancement in Carbon Dioxide Activity and Stability on Nanostructured Silver Electrode and the Role of Oxygen. *Appl. Catal., B* **2016**, *180*, 372−378.

(28) Lobaccaro, P.; Singh, M. R.; Clark, E. L.; Kwon, Y.; Bell, A. T.; Ager, J. W. Effects of Temperature and Gas-Liquid Mass Transfer on the Operation of Small Electrochemical Cells for the Quantitative Evaluation of CO_2 Reduction Electrocatalysts. *Phys. Chem. Chem. Phys.* **2016**, *18*, 26777−26785.

(29) Singh, M. R.; Kwon, Y.; Lum, Y.; Ager, J. W.; Bell, A. T. Hydrolysis of Electrolyte Cations Enhances the Electrochemical Reduction of CO_2 over Ag and Cu. *J. Am. Chem. Soc.* **2016**, *138*, 13006−13012.

(30) Thorson, M. R.; Siil, K. I.; Kenis, P. J. a. Effect of Cations on the Electrochemical Conversion of CO_2 to CO. *J. Electrochem. Soc.* **2013**, *160*, F69−F74.

(31) Murata, A.; Hori, Y. Product Selectivity Affected by Cationic Species in Electrochemical Reduction of CO_2 and CO at a Cu Electrode. *Bull. Chem. Soc. Jpn.* **1991**, *64*, 123−127.

(32) Hori, Y.; Suzuki, S. Electrolytic Reduction of Carbon Dioxide at Mercury Electrode in Aqueous Solutions. *Bull. Chem. Soc. Jpn.* **1982**, *55*, 660−665.

(33) Pocker, Y.; Bjorkquist, D. W. Stopped-Flow Studies of Carbon Dioxide Hydration and Bicarbonate Dehydration in Water and Water-d2. Acid-Base and Metal Ion Catalysis. *J. Am. Chem. Soc.* **1977**, *99*, 6537−6543.

(34) Lobaccaro, P.; Singh, M. R.; Clark, E. L.; Kwon, Y.; Bell, A. T.; Ager, J. W. Effects of Temperature and Gas−liquid Mass Transfer on the Operation of Small Electrochemical Cells for the Quantitative Evaluation of CO_2 Reduction Electrocatalysts. *Phys. Chem. Chem. Phys.* **2016**, *18*, 26777−26785.

(35) Gupta, N.; Gattrell, M.; MacDougall, B. Calculation for the Cathode Surface Concentrations in the Electrochemical Reduction of CO_2 in $KHCO_3$ Solutions. *J. Appl. Electrochem.* **2006**, *36*, 161−172.

(36) Dutta, A.; Rahaman, M.; Luedi, N. C.; Mohos, M.; Broekmann, P. Morphology Matters: Tuning the Product Distribution of CO_2 Electroreduction on Oxide-Derived Cu Foam Catalysts. *ACS Catal.* **2016**, *6*, 3804−3814.

(37) Schouten, K. J. P.; Kwon, Y.; van der Ham, C. J. M.; Qin, Z.; Koper, M. T. M. A New Mechanism for the Selectivity to C_1 and C_2 Species in the Electrochemical Reduction of Carbon Dioxide on Copper Electrodes. *Chem. Sci.* **2011**, *2*, 1902.

(38) Hori, Y.; Wakebe, H.; Tsukamoto, T.; Koga, O. Adsorption of CO Accompanied with Simultaneous Charge Transfer on Copper

DOI: 10.1021/acs.jpcc.7b03673
J. Phys. Chem. C 2017, 121, 14191−14203

Single Crystal Electrodes Related with Electrochemical Reduction of CO_2 to Hydrocarbons. *Surf. Sci.* **1995**, *335*, 258−263.
(39) Feng, X.; Jiang, K.; Fan, S.; Kanan, M. W. A Direct Grain-Boundary-Activity Correlation for CO Electroreduction on Cu Nanoparticles. *ACS Cent. Sci.* **2016**, *2*, 169−174.
(40) Handoko, A. D.; Ong, C. W.; Huang, Y.; Lee, Z. G.; Lin, L.; Panetti, G. B.; Yeo, B. S. Mechanistic Insights into the Selective Electroreduction of Carbon Dioxide to Ethylene on Cu_2O-Derived Copper Catalysts. *J. Phys. Chem. C* **2016**, *120*, 20058−20067.
(41) Singh, M. R.; Clark, E. L.; Bell, A. T. Effects of Electrolyte, Catalyst, and Membrane Composition and Operating Conditions on the Performance of Solar-Driven Electrochemical Reduction of Carbon Dioxide. *Phys. Chem. Chem. Phys.* **2015**, *17*, 18924−18936.
(42) Kas, R.; Kortlever, R.; Yılmaz, H.; Koper, M. T. M.; Mul, G. Manipulating the Hydrocarbon Selectivity of Copper Nanoparticles in CO_2 Electroreduction by Process Conditions. *ChemElectroChem* **2015**, *2*, 354−358.
(43) Schouten, K. J. P.; Qin, Z.; Gallent, E. P.; Koper, M. T. M. Two Pathways for the Formation of Ethylene in CO Reduction on Single-Crystal Copper Electrodes. *J. Am. Chem. Soc.* **2012**, *134*, 9864−9867.
(44) Schouten, K. J. P.; Pérez Gallent, E.; Koper, M. T. M. The Influence of pH on the Reduction of CO and to Hydrocarbons on Copper Electrodes. *J. Electroanal. Chem.* **2014**, *716*, 53−57.
(45) Goodpaster, J. D.; Bell, A. T.; Head-Gordon, M. Identification of Possible Pathways for C−C Bond Formation during Electrochemical Reduction of CO_2: New Theoretical Insights from an Improved Electrochemical Model. *J. Phys. Chem. Lett.* **2016**, *7*, 1471−1477.
(46) Xiao, H.; Cheng, T.; Goddard, W. A.; Sundararaman, R. Mechanistic Explanation of the pH Dependence and Onset Potentials for Hydrocarbon Products from Electrochemical Reduction of CO on Cu (111). *J. Am. Chem. Soc.* **2016**, *138*, 483−486.
(47) Tang, W.; Peterson, A. A.; Varela, A. S.; Jovanov, Z. P.; Bech, L.; Durand, W. J.; Dahl, S.; Norskov, J. K.; Chorkendorff, I. The Importance of Surface Morphology in Controlling the Selectivity of Polycrystalline Copper for CO_2 Electroreduction. *Phys. Chem. Chem. Phys.* **2012**, *14*, 76−81.

DOI: 10.1021/acs.jpcc.7b03673
J. Phys. Chem. C 2017, 121, 14191−14203